Supplementary Information

Motion-resilient and rapid contactless heart rate monitoring by overcoming dual physical barriers

Zengdi Bao[1, 2], Ningning Wu[1,2], Jiahao Zhu[1,2], Zhenhao Yang[1,2], Yang Li[1,3,4], Cheng Hu[1], and Yanhua Wang[1,3,4]

[1]Radar Technology Research Institute, Beijing Institute of Technology, Beijing 100081, China. [2]Yangtze Delta Region Academy, Beijing Institute of Technology, Jiaxing, Zhejiang 314019, China. [3]Zhengzhou Academy of Intelligent Technology, Beijing Institute of Technology, Zhengzhou, 450000, China. [4]Henan Provincial Center for Integrated Innovation in Advanced Radar Intelligent Sensing, Zhengzhou, 450000, China. e-mail: zdbao@bit.edu.cn; wyhlucky@bit.edu.cn.

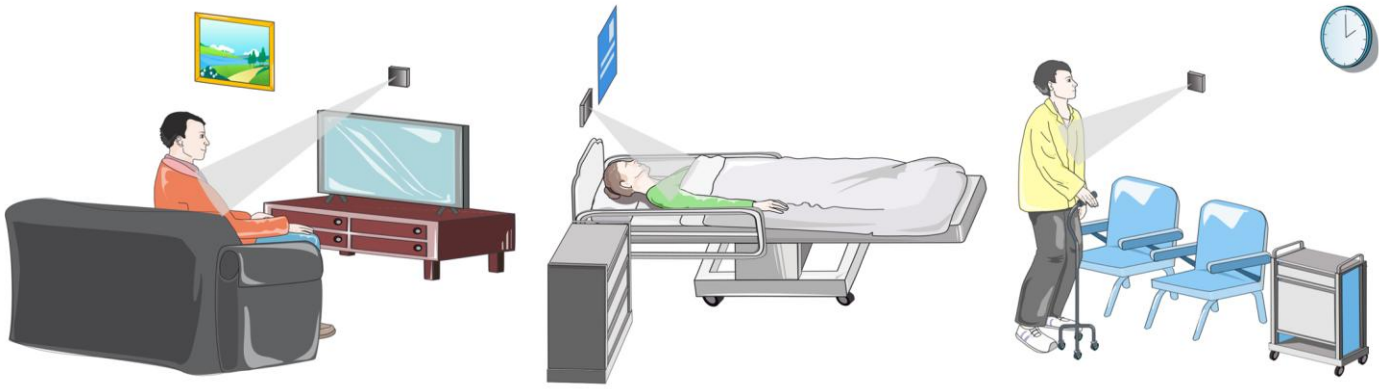

Supplementary Fig. 1 | Practical deployment environments for contactless vital sign monitoring. Typical applications include residential homes, clinical wards, and nursing facilities. In these unconstrained scenarios, the radar beam typically intersects the subject's torso at an oblique angle. This specific geometric configuration naturally forces the localized heartbeat and broader respiration signals to occupy distinct spatial range bins.

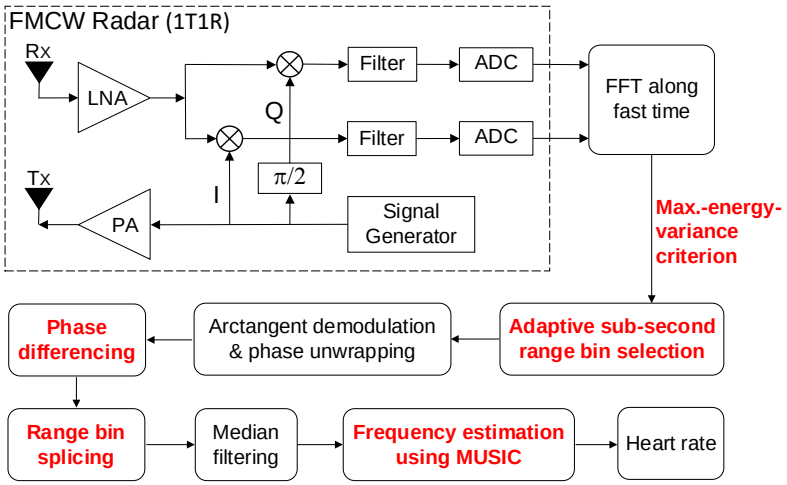

Supplementary Fig. 2 | Hardware and processing pipeline. Block diagram of the hardware configuration and signal processing pipeline. Note that only a single transmit/receive pair (1T1R) was activated. **Tx**, transmitter; **Rx**, receiver; **PA**, power amplifier; **LNA**, low noise amplifier; **ADC**, analog-to-digital converter.

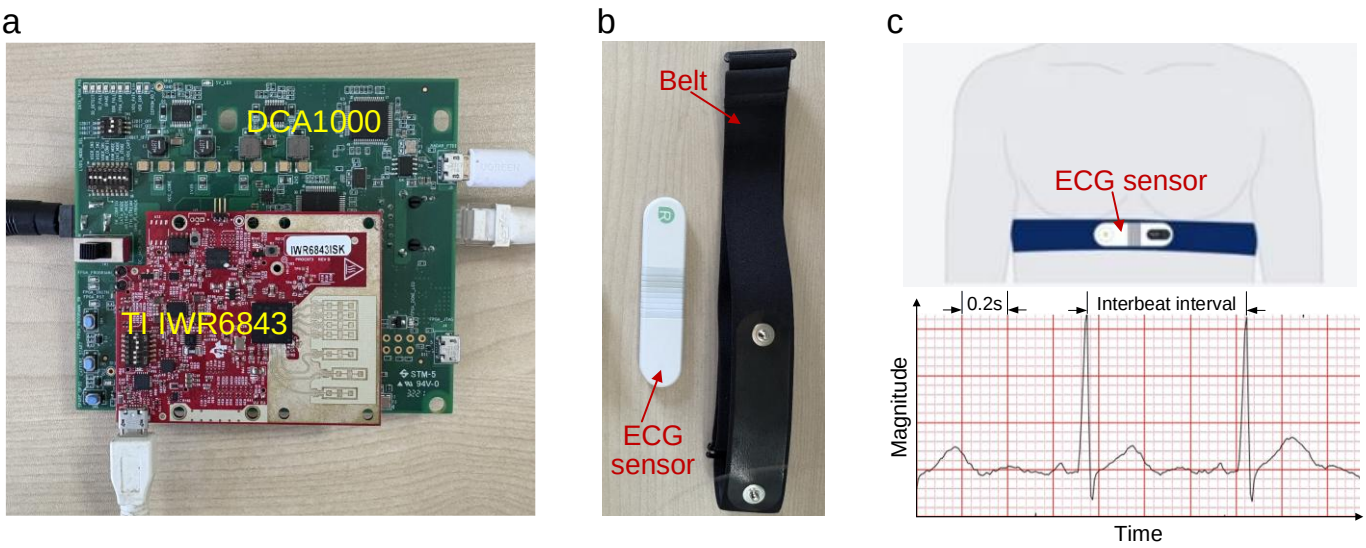

Supplementary Fig. 3 | Hardware configuration for experimental data collection. a, Radar transceiver system. The commercial TI IWR6843 millimeter-wave radar board, strictly operated in a single-transmit, single-receive (1T1R) mode, paired with a DCA1000 real-time data capture card. **b,** Ground-truth reference sensor. The wearable electrocardiogram (ECG) sensor and accompanying chest belt used to validate radar measurements. **c,** In vivo application. The ECG sensor is positioned underneath the subject's clothing; beat-to-beat heart rates were directly computed from the interbeat (R-R) intervals of these recorded waveforms.

Supplementary Table 1 | Overall estimation errors under varying windowing configurations. The overall MAPE of the measured heart rates for stationary and motion conditions. For each condition, 25 independent one-minute trials were conducted across five volunteers, comprising five separate runs per participant.

Window length		Overall MAPE (%)	
Range bin selection	**Frequency estimation**	**Stationary**	**Motion**
0.05s	1s	12.8	11.6
	3s	8.5	7.8
	5s	6.7	7.1
0.5s	1s	13.1	11.4
	3s	10.7	8.2
	5s	10.2	8.5
1s	1s	12.7	11.8
	3s	11.8	8.9
	5s	10.4	8.7
2s	2s	15.0	10.5
	3s	12.0	9.4
	5s	11.5	9.2
3s	3s	12.5	9.0
4s	4s	11.1	8.7
5s	5s	11.4	9.0

Supplementary Table 2 | Parameters for the adaptive windowing configurations. Mapping of the specific window lengths utilized for range bin selection across varying heart rate intervals. The defined heart rate thresholds dictate the bin-selection window lengths and vary systematically across each of the four configurations.

Window length (s)	Adaptive windowing configurations			
	a	b	c	d
0.05	>95	>100	>105	>110
0.2	85<HR ≤95	90<HR ≤100	95<HR ≤105	100<HR ≤110
0.5	75<HR ≤85	80<HR ≤90	85<HR ≤95	90<HR ≤100
1	≤75	≤80	≤85	≤90

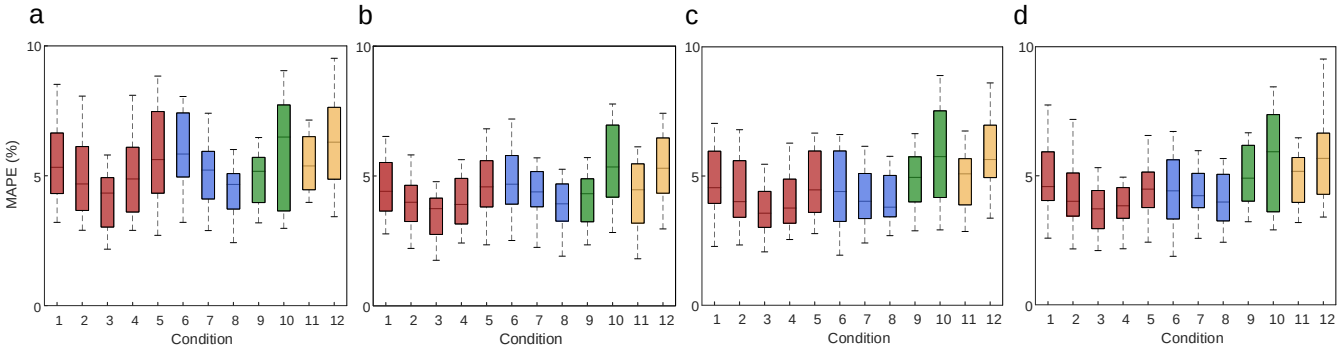

Supplementary Fig. 4 | Performance comparison of adaptive windowing configurations. a–d, Distribution of the mean absolute percentage error (MAPE) for the estimated heart rates across 12 distinct postural and motion conditions. The panels illustrate the performance outcomes derived from the four adaptive windowing configurations detailed in Supplementary Table 2. For each condition, 20 independent one-minute measurements were conducted across four participants. Each error bar represents the MAPE distribution for a specific condition under a single windowing configuration.

Supplementary Table 3 | Exact median and overall MAPE of the estimated heart rates. The tabulated values correspond to the error bar distributions shown in Supplementary Fig. 3a–d. Ultimately, configuration b was selected for the final framework.

Configuration	Median MAPE (%) for the 12 conditions												Overall MAPE (%)
	1	2	3	4	5	6	7	8	9	10	11	12	
a	5.3	4.7	4.3	4.9	5.6	5.8	5.2	4.7	5.2	6.5	5.4	6.3	5.3
b	4.4	4.0	3.7	3.9	4.6	4.7	4.4	3.9	4.3	5.4	4.5	5.3	4.4
c	4.6	4.0	3.6	3.8	4.5	4.4	4.0	3.8	5.0	5.8	5.1	5.6	4.5
d	4.6	4.0	3.7	3.9	4.5	4.4	4.2	4.0	4.9	5.9	5.2	5.7	4.6

Supplementary Table 4 | Impact of frequency-estimation window length on heart rate accuracy. MAPE evaluated under both stationary and motion conditions. For each condition, 50 independent one-minute trials were conducted across 10 volunteers.

Frequency-estimation window length	MAPE (%)	
	Stationary	Motion
3 s	5.5	7.0
5 s	4.5	4.9

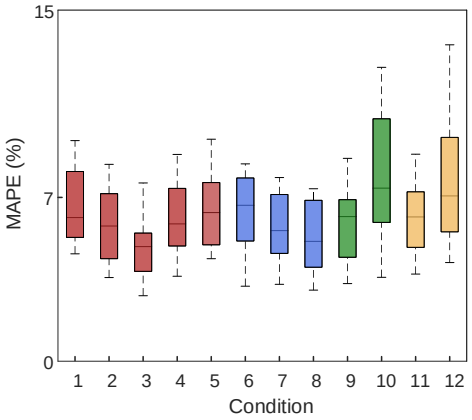

Supplementary Fig. 5 | Performance evaluation of a 3-second frequency-estimation window. MAPE of the estimated heart rates across all 12 postural and motion conditions, utilizing a 3 s frequency-estimation configuration. For each condition, 20 independent one-minute measurements were conducted across four participants.

Supplementary Table 5 | Impact of frequency-estimation window length on heart rate accuracy. Median and overall MAPE across all 12 postural and motion conditions, evaluated using 3 s and 5 s frequency-estimation windows (corresponding to Supplementary Fig. 4 and Supplementary Fig. 3b, respectively).

Frequency-estimation window length	Median MAPE (%)for the 12 conditions												Overall MAPE (%)
	1	2	3	4	5	6	7	8	9	10	11	12	
3 s	6.1	5.8	4.9	5.9	6.4	6.7	5.6	5.1	6.2	7.4	6.2	7.1	6.1
5 s	4.4	4.0	3.7	3.9	4.6	4.7	4.4	3.9	4.3	5.4	4.5	5.3	4.4